Anti-collision Device of DSTWR and SFKF Hybrid Positioning Vehicle

AnHua Wang(✉), HongKai Ding, and DongDong Wan

Electronic and Information Engineering Institute, Heilongjiang University of Science and Technology, Harbin 150022, China
3036361_cn@sina.com

Abstract. In order to suppress the hidden danger brought by the blind area of construction vehicles, a vehicle collision prevention device is designed. The realization method is introduced in the paper. Combined with DSTWR and SFKF algorithm, UWB detection technology is applied to achieve reliable ranging and positioning. It is found through one-to-many ranging experiment that the maximum static absolute error is 0.093 m, the average static error is 0.37 m, and the maximum static relative error is 0.0106; the maximum dynamic absolute error is 0.15 m, the average dynamic error is 0.073 m, and the maximum dynamic relative error is 0.0174. The positioning experiment shows that the maximum errors along the direction of the three axes are 0.17 m, 0.29 m, and 0.45 m, and the average position error of the node is about 0.241 m. The experimental results show that the proposed method satisfies the actual functional requirements, and can ensure stable detection with high speed and accuracy. The large error and track discontinuity under the action of motion and vibration factors can be effectively suppressed by the method, which has application value.

Keywords: Anti-collision of the vehicle · Ultra-wideband · Positioning · Kalman filter

1 Introduction

With the continuous improvement of industrial mechanization, engineering vehicles are widely used in the construction of ports, mines, road, bridge and so on. There are blind spots for many engineering vehicles in the operation process, making a personal safety hazard for on-site construction personnel. Therefore, it is of great significance to develop a wireless ranging and positioning system with automatic detection and early warning functions [1–3].

At present, more mature ranging methods include laser, microwave, infrared, GPS and ultrasonic. The basic principles of laser, ultrasonic and infrared measurement distances are: The target sends laser, ultrasonic or infrared light, and the receiver sends them by the original way. And then the time interval between transmission and reception is obtained to estimate the distance. Laser ranging must be point-to-point ranging, and

X. Jiang and P. Li (Eds.): GreeNets 2020, LNICST 333, pp. 94–107, 2020.
https://doi.org/10.1007/978-3-030-62483-5_11

ultrasonic and infrared ranging are easily affected by multipath environments, resulting in low accuracy [4, 5]. A microwave with a carrier wavelength of 0.8–10 cm is used to achieve microwave ranging, and it is modulated and transmitted by the primary station, received and forwarded via the secondary station. The post-lag phase difference of the modulated wave after mixing processing is measured to estimate the distance. The cost of microwave ranging is high [6, 7]. Based on the global positioning system and the Beidou positioning system, GPS ranging is combined with an electronic map and road data to achieve ranging [8]. Existing GPS navigation systems are affected by complex environments. For example, accurate location services cannot be provided in viaducts and tunnel areas [9, 10]. Affected by various factors, these ranging methods have the defects, such as low immunity, high signal transmission power, channel fading, and low energy efficiency. They are not suitable for application between construction vehicles and construction personnel and construction equipment [11, 12].

In recent years, UWB communication technology has developed rapidly. UWB communication has the advantages of low power consumption, wide bandwidth, low spectral density, high data transmission rate, strong confidentiality, high multi-path immunity and high resolution [13]. How to apply UWB to achieve accurate and reliable ranging has become a research hotspot, where the ranging algorithm and signal collision avoidance mechanism are the keys [14]. TOA, TDOA, AOA, RSSI, and TWR and so on are common ranging algorithms [15–18].

The waveform characteristics of numerous UWB signals are analyzed by Stefano M and Wymeersch H et al. NLOS state identification and error reduction are carried out using support vector machine to effectively eliminate NLOS error and improve ranging accuracy. However, this method is based on a large number of data statistics with a large workload; Huerta J M et al. use particle filter and unscented Kalman filter to locate position and measure speed, which can effectively suppress NLOS error. However, the algorithm is too complicated to implement [19, 20]; in the literature [21], ranging is achieved by integrating RTT (Round Trip Time) and AOA (Angle Of Arrival) to propose a grid-based clustering algorithm that does not need to master the prior conditions such as the indoor environment. However, its hardware part should be based on the antenna array, with a high cost; literature [22] judges the NLOS state based on the prior information, and identifies the NLOS error by INS (Inertial Navigation System) and processes it. Since this method is more complicated, the additional hardware is required.

In order to improve the reliability of measurement information, the theory of robust estimation is proposed by Yang Y X et al. to eliminate measurement error[19]. Combined neural network and Kalman filtering, adaptive suppression state vector and measurement interference method are proposed by Gao Weiguang and others. But the training process of the neural network has a large workload [23, 24]. A new vector robustness factor is proposed by Miao Yuewang et al. using the GNSS/INS combination to improve the system accuracy [25, 26].

Considering the system detection speed, accuracy and reliability requirements under actual working conditions, the combination of DSTWR (Double-sided Two-way Ranging) algorithm and SFKF (Sampling Fitting Robust Kalman Filter) is proposed to achieve ranging and positioning [27].

2 Ranging Method

DSTWR algorithm based on the improvement of TWR does not need to consider the synchronization problem between nodes in the ranging process and has higher precision and speed in the actual measurement [1]. The DSTWR ranging diagram is shown in Fig. 1.

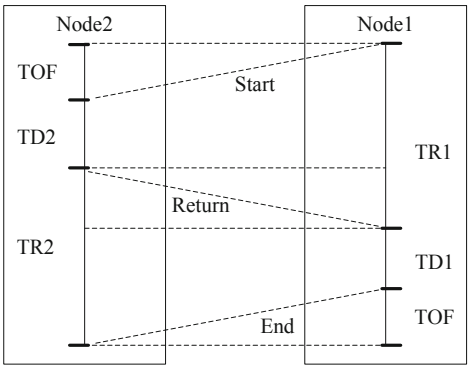

Fig. 1. Ranging principle diagram of DSTWR.

Node 1 sends a Start signal to Node 2. After a T_{D2} time, node 2 sends a Return signal to node 1. After a T_{D1} time, node 1 sends an End signal to node 2. Supposing that time interval of sending and receiving of node 1 is T_{R1}, and that time interval of sending and receiving of node 2 is T_{R2}, and the flight time between the two nodes is TF, it can be obtained that:

$$T_{R1} = 2T_F + T_{D2} \tag{1}$$

$$T_{R2} = 2T_F + T_{D1} \tag{2}$$

Simultaneous formula (1) and (2), the flight time is:

$$\begin{aligned} T_F &= \frac{T_F(2T_{D2} + 4T_F + 2T_{D1})}{2T_{D2} + 4T_F + 2T_{D1}} \\ &= \frac{T_F(2T_{D2} + 4T_F + 2T_{D1})}{T_{R2} + T_{R1} + T_{D2} + T_{D1}} \\ &= \frac{(T_{D2} + 2T_F)(T_{D1} + 2T_F) - T_{D2} \times T_{D1}}{T_{R2} + T_{R1} + T_{D2} + T_{D1}} \\ &= \frac{T_{R2} \times T_{R1} - T_{D2} \times T_{D1}}{T_{R2} + T_{R1} + T_{D2} + T_{D1}} \end{aligned} \tag{3}$$

The distance between the two nodes is:

$$d = \frac{T_{R2} \times T_{R1} - T_{D2} \times T_{D1}}{T_{R2} + T_{R1} + T_{D2} + T_{D1}} \times C \tag{4}$$

In the formula (4), C represents a signal transmission speed.

Supposing the offset errors of two node clocks are e_1 and e_2 respectively, and they are brought in the Eq. (4) to obtain the actual distance d' of the two nodes:

$$d' = \frac{T_{R2}(1 + e_2) \times T_{R1}(1 + e_1) - T_{D2}(1 + e_2) \times T_{D1}(1 + e_1)}{T_{R2}(1 + e_2) + T_{R1}(1 + e_1) + T_{D2}(1 + e_2) + T_{D1}(1 + e_1)} \times C \quad (5)$$

The distance error Δd of the simultaneous Eqs. (4) and (5) is:

$$\Delta d = d - d' = (T_F(e_1 - e_2) + T_F \times O(e_1, e_2, T_{D2}, T_{R2})) \times C \quad (6)$$

It can be seen that the DSTWR algorithm does not need to consider the node synchronization problem, with small calculation amount and small error, which can ensure the high measurement accuracy and speed [28, 29].

3 Location Method

Positioning is the extension of point-to-point ranging, which is achieved by measuring the distance from a node to multiple base stations [30]. The distance value during the positioning process is sent to the upper computer, and the upper computer calculates the distance according to the distance from the node to all the base stations, as shown in Fig. 2. Taking the three base stations as an example, the coordinates of the three base stations are known, the coordinates of each base station are taken as the origin point, draw three circles based on the distance from the node to each base stations, and the intersection point of the three circles is node coordinates [31–33].

Due to external noise interference, when the positioning node is in the moving state, the measured node movement trajectory is intermittent [34]. Considering the requirements of algorithm accuracy, speed and complexity in practical applications [35], the Kalman filtering algorithm is introduced, which makes the measurement results smoothed and more in line with the movement trajectory.

Supposing the nonlinear state equation and the observation equation expression are:

$$Y(m+1) = f\left[y(m), u(m), w(m)\right] \quad (7)$$

$$G(m) = h\left[g(m), u(m), v(m)\right] \quad (8)$$

In Eqs. (7) and (8), $f[\cdot]$ represents the transition function of the nonlinear state, $w(m)$ represents the noise component, $h[\cdot]$ represents a nonlinear observation function, $v(m)$ represents an observed noise component. Both variable $w(m)$ and variable $v(m)$ are Gaussian white noise, and the variances are respectively Q and R. $Y(m+1)$ is the state vector, $g(m)$ is the observation vector and $u(m)$ is the control vector. According to the Gaussian distribution, the recursion relationship of the state variable $Y_{m,m}$ and $Y_{m,m-1}$ at time m is:

$$\hat{Y}_{m,m} = \hat{Y}_{m,m-1} + A_m \cdot (G_m - \hat{G}_m) \quad (9)$$

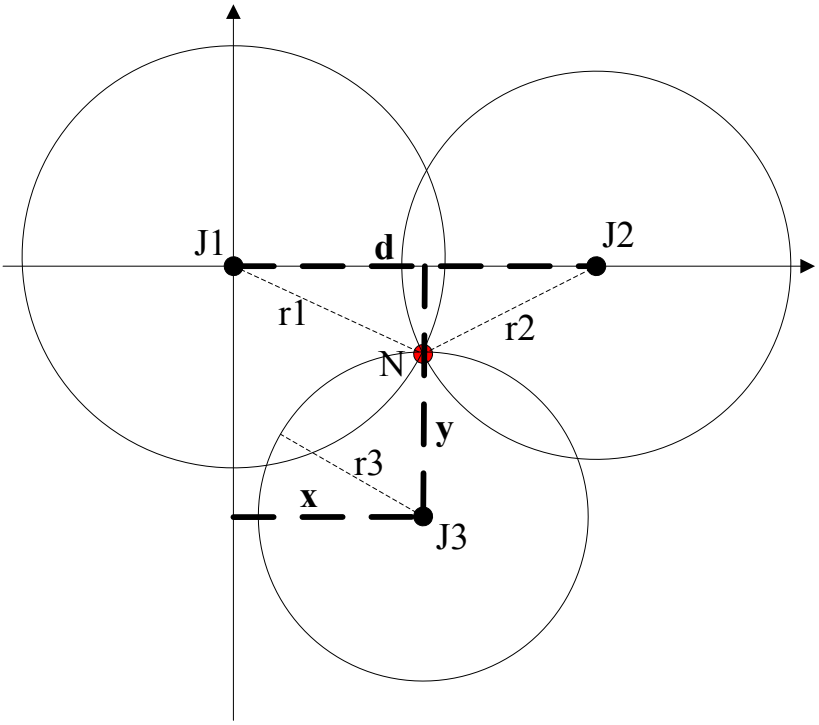

Fig. 2. Three base stations positioning principle.

In Eq. (9), A_m is the denoising gain, $Y_{m,m-1}$ is the previous state value and G_m is the optimal prediction value. System updates and forecasts can be expressed as:

$$\begin{aligned} A_m &= P_{y_m g_m} \cdot P_{g_y}^{-1} \\ P_m &= P_{m,m-1} - A_m \cdot P_{g_m} A_m^T \\ \hat{Y} &= \hat{Y}_{m,m-1} + A_m \cdot (G_m - \hat{G}_m) \end{aligned} \tag{10}$$

The Jacobian linearization matrix can be expressed as:

$$\begin{aligned} \phi_{m,m-1} &= \frac{\partial f[y_{m-1}, w_{m-1}]}{\partial y_{m-1}} | y_{m-1} = \hat{y}_{m-1} \\ H_m &= \frac{\partial h[y_m, v_m]}{\partial y_m} | y_m = f(\hat{y}_{m-1}, w_{m-1}) \end{aligned} \tag{11}$$

The Eq. (10) and (11) are substituted into Eq. (7):

$$\begin{aligned} &\hat{y}_m = f(\hat{y}_{m,m-1}, w_{m-1}) + A_m \cdot \{g_m - h_m[f(\hat{y}_{m-1}, w_{m-1}, v_m)]\} \\ &A_m = P_{m,m-1} \cdot H_m^T \cdot (H_m \cdot P_{m,m-1} \cdot H_m^T \cdot R_m)^{-1} \\ &P_{m,m-1} = \phi_{m,m-1} \cdot P_{m-1} \cdot \phi_{m,m-1}^T + Q_{m-1} \\ &P_m = (I - A_m \cdot H_m) \cdot P_{m,m-1} \\ &\hat{y}_0 = E[y_0],\ P_0 = E[(y_0 - \hat{y}_0)(y_0 - \hat{y}_0)^T] \end{aligned} \tag{12}$$

Equation (12) belongs to the state recursion equation, the initial value determines the accuracy of the prediction result, and the high precision can be maintained only when

the linear equation is approximated. Therefore, the state vector is first sampled to fit the linear equation, and then filtering is carried out to make the prediction result closer to reality.

Let the state equation of a wireless sensor node be:

$$Y_{m+1} = f_m(Y_m) + W_m \tag{13}$$

The measurement equation is:

$$G_m = h_m(Y_m) + V_m \tag{14}$$

In the Eqs. (13) and (14), m represents the time m and g_m represents a measurement vector corresponding to the time m. y_m indicates the state vector at time m, h_m is the measured value, f_m represents the state transition function. w_m and v_m are zero mean white noise and they are not correlated with each other.

The sigma point sample is carried out for the state vector y. The y statistical property is $(\bar{y}, P_y)$. There are $2n + 1$ sampling points, which are respectively $\xi_i (i = 0, 1, 2, \cdots, 2n)$. The expressions of ξ and the weight ω are:

$$\begin{cases} \xi_0 = \bar{Y} \\ \xi_i = \bar{Y} + (\sqrt{(n+\lambda)P_y})_i, \ (1 \le i \le n) \\ \xi_i = \bar{Y} - (\sqrt{(n+\lambda)P_y})_i, \ (n < i \le 2n) \end{cases} \tag{15}$$

$$\begin{cases} \omega_0^{(jz)} = \frac{\lambda}{\lambda+n} \\ \omega_i^{(jz)} = \frac{0.5}{\lambda+n}, (i = 1, 2, \ldots, 2n) \end{cases} \tag{16}$$

$$\begin{cases} \omega_0^{(fc)} = \frac{\lambda}{\lambda+n} + (1 - \alpha^2 + \beta) \\ \omega_i^{(fc)} = \frac{0.5}{\lambda+n}, (i = 1, 2, \cdots, 2n) \end{cases} \tag{17}$$

In Eqs. (15)–(17), λ is the scaling factor of the sampling point and mean spacing. Supposing $\lambda = \alpha^2(n + l) - n$, l generally takes 0. α usually takes 0.1, indicating the degree of dispersion of the sampling points; $(\sqrt{(n+\lambda)P_y})_i$ corresponds to the ith column square root of the matrix; β takes 2 (consistent with Gaussian distribution) and describe the distribution information of y; $\omega^{(jz)}$ represents the mean weight value and $\omega^{(fc)}$ represents the variance weight value.

The prediction function of the node state is:

$$\begin{cases} \xi^i_{m|m-1} = f_m(\xi^{(i)}_{m-1|m-1}), \ i = 0, 1, 2, \cdots, 2n \\ \hat{y}_{m|m-1} = \sum_{i=0}^{2n} \omega_i^{(jz)} \xi^{(i)}_{m|m-1} \\ P^{(i)}_{m|m-1} = \sum_{i=0}^{2n} \omega_i^{(fc)} (\xi^{(i)}_{m|m-1} - \hat{y}_{m|m-1})(\xi^{(i)}_{m|m-1} - \hat{y}_{m|m-1})^T + Q_{m-1} \end{cases} \tag{18}$$

The prediction function of node measurement is:

$$\begin{cases} \zeta_{m|m-1}^{(i)} = h_m(\xi_m^{(i)}), i = 0, 1, 2, \cdots, 2n \\ \hat{g}_{m|m-1} = \sum_{i=0}^{2n} \omega_i^{(jz)} \zeta_{m|m-1}^{(i)} \\ P_{\hat{y}_m} = \sum_{i=0}^{2n} \omega_i^{(fc)} (\zeta_{m|m-1}^{(i)} - \hat{y}_{m|m-1})(\zeta_{m|m-1}^{(i)} - \hat{y}_{m|m-1})^T + R_m \\ P_{\hat{y}_m \hat{g}_m} = \sum_{i=0}^{2n} \omega_i^{(fc)} (\zeta_{m|m-1}^{(i)} - \hat{y}_{m|m-1})(\zeta_{m|m-1}^{(i)} - \hat{y}_{m|m-1})^T \end{cases} \tag{19}$$

The update of the covariance matrix and the Kalman coefficient K of the node state prediction can be expressed as:

$$\begin{cases} \hat{y}_{m|m} = \hat{y}_{m|m-1} + K_m(g_m - \hat{g}_{m|m-1}) \\ K_m = P_{\bar{y}_m \bar{g}_m} P_{\bar{g}_m}^{-1} \\ P_{m|m} = P_{m|m-1} - K_m P_{\bar{g}_m} K_m^T \end{cases} \tag{20}$$

According to Eqs. (15)–(20), the nodes' position estimates of every moment can be obtained.

Supposing the node coordinate is $y = (x, y)^T$ and state vector is $y_m = (x_m, y_m)^T$, then the state equation is:

$$y_{m+1} = D y_m + w_m \tag{21}$$

In Eq. (21), w_m represents noise and D represents a state transition matrix (unit matrix).

The quantity measurement model varies with the observed value, base station node is supposed to be $n(n = 1, 2, 3)$. L_m is a three-dimensional distance vector, and v_m is three-dimensional noise. When the observed value is the distance between the base station and a node, the measurement function is:

$$\begin{cases} g_m = L_m = h_m(y_m) + v_m \\ L_m = \begin{pmatrix} L_{m1} \\ L_{m2} \\ L_{m3} \end{pmatrix} = \begin{pmatrix} \sqrt{(x_m - x_{n1})^2 + (y_m - y_{n1})^2} \\ \sqrt{(x_m - x_{n2})^2 + (y_m - y_{n2})^2} \\ \sqrt{(x_m - x_{n3})^2 + (y_m - y_{n3})^2} \end{pmatrix} \end{cases} \tag{22}$$

In Eq. (22), $L = (L_1 L_2 L_3)^T$ is the distance from a node to the base station, $L_m = (L_{m1} L_{m2} L_{m3})^T$ is the distance vector at the mth calculation. $x_{n1} = (x_{n1}, y_{n1})^T$, $x_{n2} = (x_{n2}, y_{n2})^T$ and $x_{n3} = (x_{n3}, y_{n3})^T$ are respectively the coordinate vector of the base station $n(n = 1, 2, 3)$.

4 Construction of Hardware Experiment Platform

The wireless ranging and positioning system is a wireless network composed of a plurality of base station devices and a plurality of node devices. The structure of each base

station or node is shown in Fig. 3, including the control unit with STM32F103C8T6 as the core, DWM1000 communication unit, alarm unit, and power supply unit. The power supply unit of the base station is composed of USB interface and voltage regulator chip, and the power supply unit of the node is composed of USB interface, voltage conversion module, battery and charging management module.

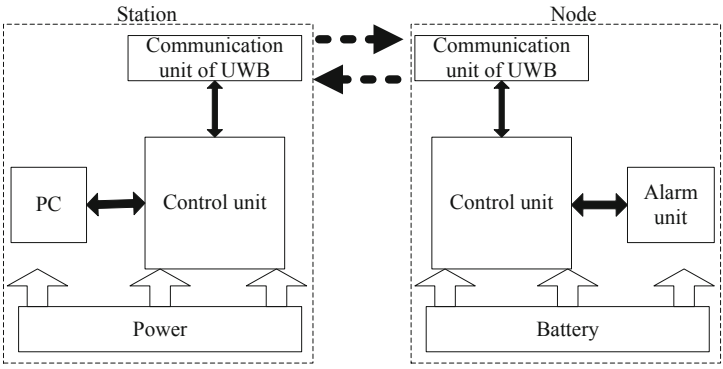

Fig. 3. Structure diagram base station (node).

Each base station and node has a unique code. Each base station and the node can communicate wirelessly. The base station detects and calculates the distance of each node, and the alarm can be triggered when the detected distance value exceeds the safe range. The measurement results of multiple base stations can be referred to locate the node. The control unit mainly completes the work such as timing provision, distance calculation and control instruction release for the UWB unit; with UWM data transceiving function, the communication unit can accurately measure time stamps [36].

5 Test Experiment

Ranging experiment and positioning experiment are carried out respectively according to the anti-collision alarm function, detection accuracy, speed demand, simulation system application environment. First, a base station and four nodes are used to perform basic system function tests, that is distance detection between the base station and each node. The notebook is connected to the base station by using the serial port, and the operation results of the base station at two times are randomly selected as shown in Fig. 4(a) and Fig. 4(b). The selected node numbers are node [1], node [2], node [3], and node [4], respectively. Therefore, dist[1], dist[2], dist[3], and dist[4] in Fig. 4(a) and Fig. 4(b) respectively represent the distance values from the base station to the four nodes, which are in centimeters. So the system is able to provide valid data for test experiments. Before each test, the distance from the base station to the node must be calibrated.

5.1 Static Ranging Experiment

A square is selected as a test site to simulate a working environment such as a dock and a distribution center, and place a base station in the car body. Considering the actual

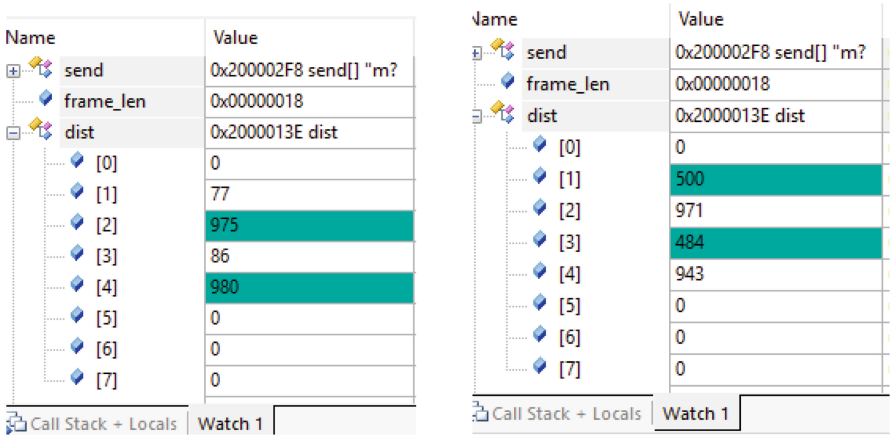

(a) result(1) (b) results(2)

Fig. 4. Base station operation.

application, 12 m, 10 m and 8 m are respectively set as alarm thresholds, and correspond to different alarm sounds. One node is placed in turn at 12 m, 10 m, and 8 m from the car body, and stayed at each position for enough time to obtain enough experimental data. The photograph of ranging experiment is shown in Fig. 5(a), and the photograph of collision prevention device is shown in Fig. 5(b). The base station calculation results are shown in Fig. 6(a), Fig. 6(b), and Fig. 6(c). The horizontal axis represents the number of tests and the vertical axis represents the distance value. It can be seen that the maximum ranging errors of 12 m, 10 m, and 8 m are 0.089 m, 0.093 m, and 0.085 m respectively, and the average errors are 0.0374 m, 0.0380 m and 0.0349 m respectively.

(a) the ranging experiment (b) the collision prevention device

Fig. 5. The photos of physical test.

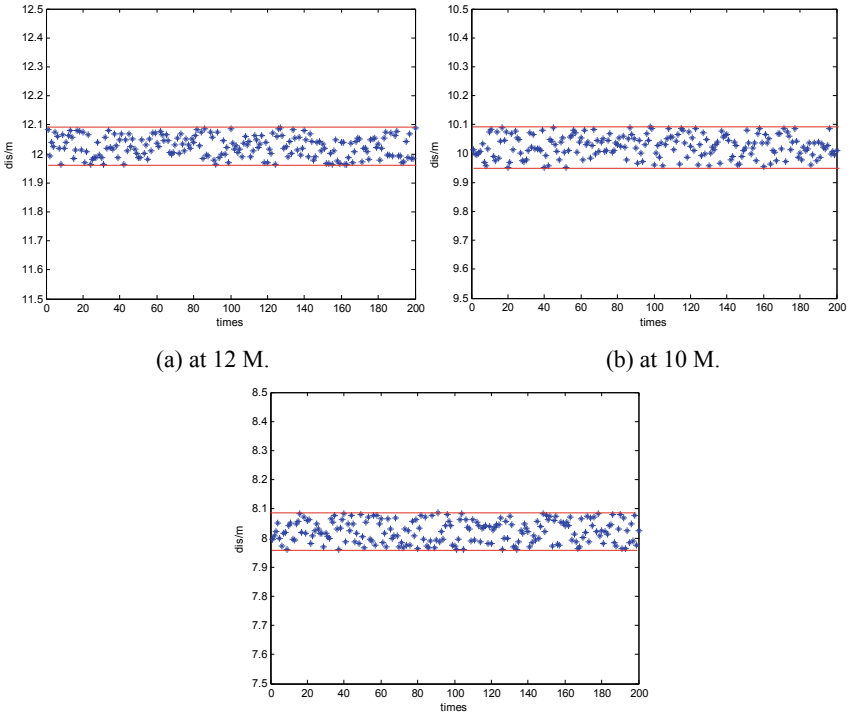

(a) at 12 M. (b) at 10 M.

(c) at 8 M.

Fig. 6. Static ranging results.

5.2 Dynamic Ranging Experiment

In order to simulate the actual working conditions, multiple vehicles are arranged around the vehicle and nodes at the base station as a signal barrier. Generally, engineering vehicles are not too fast. So the base station vehicle approaches the node at a speed of 25 km/h. The operation results of the base station are shown in Fig. 7(a), Fig. 7(b), and Fig. 7(c). The maximum ranging errors which are visible at 12 m, 10 m, and 8 m is 0.148 m\0.15 m\0.139 m, respectively. The average errors are 0.073 m, 0.075 m, and 0.070 m, respectively.

5.3 Positioning Experiment

The three base stations are respectively placed at fixed positions (at the same height, and within the effective communication distance) to form a triangular structure. The nodes are randomly moved within the effective range, and the observation positioning result and the actual position are as shown in Table 1. It can be seen that the maximum positioning errors in the three coordinate axes of X, Y and Z are 0.17 m, 0.29 m, and 0.45 m, respectively, and the average errors are 0.11 m, 0.10 m, and 0.19 m respectively.

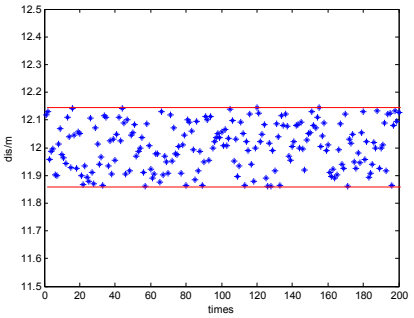

(a) at 12 M.

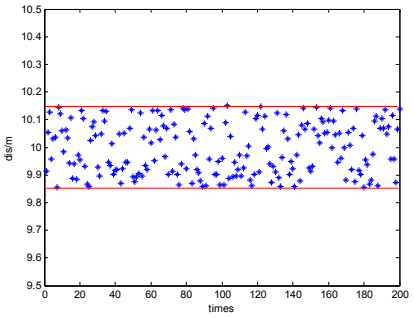

(b) at 10 M

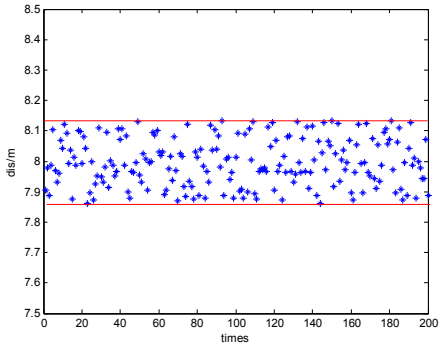

(c) at 8 M.

Fig. 7. Dynamic ranging results.

Table 1. Locating experimental results.

	Measuring coordinates/m			Actual coordinates/m			Error/m		
	X	Y	Z	X	Y	Z	ΔX	ΔY	ΔZ
1	5.06	4.97	0.98	4.99	5.01	0.85	0.07	0.04	0.13
2	5.63	9.73	0.96	5.58	9.66	0.91	0.05	0.07	0.05
3	10.8	7.54	1.06	10.7	7.52	1.24	0.12	0.02	0.18
4	8.28	7.90	0.66	8.39	8.02	0.21	0.11	0.12	0.45
5	7.35	0.83	0.47	7.18	1.12	0.78	0.17	0.29	0.31
6	3.63	1.46	0.07	3.68	1.55	0.11	0.05	0.09	0.04
7	1.98	10.2	1.86	2.13	10.2	2.09	0.15	0.01	0.23
8	0.84	3.35	0.78	0.69	3.51	0.92	0.15	0.16	0.14

6 Conclusion

The implementing method of vehicle anti-collision device is introduced in this paper. Taking DWM1000 as the core, the system achieves reliable ranging and positioning by combining DSTWR with SFKF algorithms. The test results show that the vehicle and personnel with the detection device perform different distance detection in the static state, with the maximum absolute error of 0.093 m, the average error of 0.037 m, and the maximum relative error of 0.0106; distance detection is carried out in the moving state, with the maximum absolute error of 0.15 m, the average error of 0.073 m, and the maximum relative error of 0.0174; in the positioning experiment, the maximum errors in the three coordinate axes are 0.17 m, 0.29 m, and 0.45 m, respectively, and the average position error of the node is about 0.241 m. The experimental results prove that the method in this paper can effectively eliminate large errors, stabilize the errors in small range, keep the detection track continuous, meet the actual functional requirements, and has application value. It should be noted that in practical applications, the detection algorithm and communication mechanism should be further optimized for the number of nodes.

Acknowledgment. This work was supported by Harbin Science and Technology Innovation Talents Special Project (NO. 2017RAQXJ031); Heilongjiang Fundamental Research Foundation for the Local Universities in 2018 (2018KYYWF1189); Key project Task of Public Safety Risk Control and Emergency Technical Equipment of National Key R&D Program (NO. 2017YFC0805208); 2017 National Nature Fund, (NO. 51674109).

References

1. Angelis, G.D., Moschitta, A., Carbone, P.: Positioning techniques in indoor environments based on stochastic modeling of UWB round-trip-time measurements. IEEE Trans. Intell. Transp. Syst. **17**(8), 2272–2281 (2016)
2. Abdulrahman, A., et al.: Ultra wideband indoor positioning technologies: analysis and recent advances. Sensors **16**(5), 1–36 (2016)
3. Mikhaylov, K., Petäjäjärvi, J., Hämäläinen, M., Tikanmäki, A., Kohno, R.: Impact of IEEE 802.15.4 communication settings on performance in asynchronous two way UWB ranging. Int. J. Wirel. Inf. Netw. **24**(2), 124–139 (2017). https://doi.org/10.1007/s10776-017-0340-9
4. Luo, Q., Han, B.: Distance and Azimuth testing system based on ultrasonic and infrared detecting technology. Comput. Autom. Meas. Control. **13**(4), 304–306+334 (2005)
5. Bartoletti, S., Giorgetti, A., Win, M.Z., Conti, A.: Blind selection of representative observations for sensor radar networks. IEEE Trans. Veh. Technol. **64**(4), 1388–1400 (2015)
6. Wang, D.Y., Zhao, C.F., Peng, J.Y., Li, M.: Error factors impact analysis of microwave range finder ranging accuracy. Electron. Meas. Technol. **4**, 42–44 (2010)
7. Bartoletti, S., Dai, W., Conti, A., Win, M.Z.: A mathematical model for wideband ranging. IEEE J. Sel. Top. Sig. Process. **9**(2), 216–228 (2015)
8. Yu, H.L., Guo, A.H., Luo, W.: Method of ranging based on GPS positioning data. Electron. Meas. Technol. **7**, 95–98 (2011)
9. Sangodoyin, S., Niranjan, S., Molisch, A.F.: A measurement-based model for outdoor near-ground ultrawideband channels. IEEE Trans. Antennas Propag. **64**(2), 740–751 (2016)

10. Wang, L.X., Huang, Z.G., Zhao, Y.: Term design and analysis of user range accuracy in GPS navigation message. J. Nanjing Univ. Sci. Technol. **38**(5), 620–625 (2014)
11. Zhao, X.M., Hui, F., Shi, X., Ma, J.Y., Yang, L.: Concept, architecture and challenging technologies of ubiquitous traffic information service system. J. Traffic Transp. Eng. **14**(4), 105–115 (2014)
12. Movassaghi, S., Abolhasan, M., Lipman, J., Smith, D., Jamalipour, A.: Wireless body area networks: a survey. IEEE Commun. Surv. Tutor. **16**(3), 1658–1686 (2014)
13. Xu, H.T., Chen, B., Lv, Z.G.: Modulation technology and application prospects of UWB. Inf. Technol. **4**, 175–178 (2011)
14. Wen, F., Wan, Q.: Time delay estimation based on entropy estimation. J. Electron. Sci. Technol. **11**(3), 258–263 (2013)
15. Giorgetti, A., Chiani, M.: Time-of-arrival estimation based on information theoretic criteria. IEEE Trans. Sig. Process. **61**(5–8), 1869–1879 (2013)
16. Wu, S., Li, J., Liu, S.: Single threshold optimization and a novel double threshold scheme for non-line-of-sight identification. Int. J. Commun. Syst. **27**(10), 2156–2165 (2014)
17. Fu, S.C., Li, Y.M., Zong, K., Zhang, M.J., Wu, M.: Accuracy analysis of UWB pose detection system for road-header. Chin. J. Sci. Instrument. **38**(8), 1978–1987 (2017)
18. Han, Z., He, J., Geng, Y., Xu, C., Xu, L., Duan, S.: CRLB for TOA based near-ground swarm robotic localization. In: Ubiquitous Intelligence and Computing and 2015 IEEE 12th Intl Conf on Autonomic and Trusted Computing and 2015 IEEE 15th Intl Conf on Scalable Computing and Communications and Its Associated Workshops (UIC-ATC-ScalCom), pp. 1853–1858 (2015)
19. Liu, T., Xu, A.G., Sui, X.: Adaptive robust Kalman Filtering for UWB indoor positioning. Chin. J. Sens. Actuators **31**(4), 678–686 (2018)
20. Peng, S., Chen, C., Shi, H., et al.: State of charge estimation of battery energy storage systems based on adaptive unscented Kalman Filter with a noise statistics estimator. IEEE Access **5**, 13202–13212 (2017)
21. Mao, K.J., Wu, J.B., Jin, H.B., Miao, C.Y., Xia, M., Chen, Q.Z.: Indoor localization algorithm for NLOS environment. Acta Electronica Sinica **44**(5), 1174–1179 (2016)
22. Liu, T., Xu, A.G., Sui, X.: Application of UWB/INS combination in indoor navigation and positioning. Sci. Surv. Mapp. **41**(12), 162–166 (2016)
23. Gao, W., Chen, G.: Integrated GNSS/INS navigation algorithms combining adaptive filter with neural network. Geomat. Inf. Sci. Wuhan Univ. **39**(11), 1323–1328 (2014)
24. Taran, S., Nitnaware, D.: Performance evaluation of 802.15.3a UWB channel model with antipodal, orthogonal and DPSK modulation scheme. Int. J. Microw. Wirel. Technol. **6**(1), 34–42 (2015)
25. Miao, Y.W., Zhou, W., Tian, L., et al.: Extended robust Calman filtering detection and its application based on innovation x ~ 2. Geomat. Inf. Sci. Wuhan Univ. **41**(2), 269–273 (2016)
26. Kok, M., Hol, J.D., Schön, T.B.: Indoor positioning using ultrawideband and inertial measurements. IEEE Trans. Veh. Technol. **64**(4), 1293–1303 (2015)
27. Zhang, S., Pedersen, G.F.: Mutual coupling reduction for UWB MIMO antennas with a wideband neutralization line. IEEE Antennas Wirel. Propag. Lett. **15**, 166–169 (2016)
28. Ding, H., Liu, W., Huang, X., Zheng, L.: First path detection using rank test in IR UWB ranging with energy detection receiver under harsh environments. IEEE Commun. Lett. **17**(4), 761–764 (2013)
29. Yu, K., Dutkiewicz, E.: NLOS identification and mitigation for mobile tracking. IEEE Trans. Aerosp. Electron. Syst. **49**(3), 1438–1452 (2013)
30. Angelis, A.D., Dwivedi, S., Händel, P.: Characterization of a flexible UWB sensor for indoor localization. IEEE Trans. Instrum. Meas. **62**(5), 905–913 (2013)

31. Okamoto, E., Horiba, M., Nakashima, K., Shinohara, T., Matsumura, K.: Particle swarm optimization-based low-complexity three-dimensional UWB localization scheme. In: Sixth International Conference on Ubiquitous and Future Networks. pp. 120–124 (2014)
32. Ershadh, M.: Study of the design evolution of an antenna and its performance for UWB communications. Microw. Opt. Technol. Lett. **57**(1), 81–84 (2015)
33. Zhang, Z., Zhu, J., Ruan, J., Song, G.: Distance measurement for the indoor WSN nodes using WTR method. Int. J. Distrib. Sens. Netw. **1**, 1–13 (2014)
34. Ojaroudi, N.: Compact UWB monopole antenna with enhanced bandwidth using rotated L-shaped slots and parasitic structures. Microw. Opt. Technol. Lett. **56**(1), 175–178 (2014)
35. Demir, U., Bas, C.U., Ergen, S.C.: Engine compartment UWB channel model for intravehicular wireless sensor networks. IEEE Trans. Veh. Technol. **63**(6), 2497–2505 (2014)
36. Richardson, P., Xiang, W., Shan, D.: UWB outdoor channel environments: analysis of experimental data collection and comparison to IEEE 802.l5.4a UWB channel model. Int. J. Ultra Wideband Commun. Syst. **3**(1), 1–7 (2014)